DOI 10.1007/s11595-015-1120-y

Electrochemical Hydrogen Storage Performances of the Si Added La-Mg-Ni-based A_2B_7-type Electrode Alloys for Ni/MH Battery Application

ZHANG Yanghuan[1,2], YANG Tai[2], CHEN Licui[1,2], XU Chao[1,2], REN Huiping[1], ZHAO Dongliang[2]

(1. Key Laboratory of Integrated Exploitation of Baiyun Obo Multi-Metal Resources, Inner Mongolia University of Science and Technology, Baotou 014010, China; 2. Department of Functional Material Research, Central Iron and Steel Research Institute, Beijing 100081, China)

Abstract: The casting and annealing technologies were applied to fabricate the $La_{0.8}Mg_{0.2}Ni_{3.3}Co_{0.2}Si_x$ (x = 0-0.2) electrode alloys. The effects of Si content and annealing temperature on the structure and electrochemical performances of the alloys were investigated systematically. The analyses of XRD and SEM show that all the alloys possess a multiphase structure, involving two main phases $(La, Mg)_2Ni_7$ and $LaNi_5$ as well as a residual phase $LaNi_3$. The addition of Si brings on an evident increase in the $LaNi_5$ phase and a decrease in the $(La, Mg)_2Ni_7$ phase, without altering the main phase component of the alloy, which also makes the lattice constants and cell volumes of the alloy enlarged. Likewise, the annealing treatment engenders the same action on the lattice constants and cell volumes as adding Si. Simultaneously, it gives rise to the variation of the phase abundance and the coarsening of the alloy grains. The electrochemical measurements indicate that the addition of Si ameliorates the cycle stability of the as-cast and annealed alloys significantly, but impairs their discharge capacities clearly. Similarly, the annealing treatment makes a positive contribution to the cycle stability of the alloy evidently, and the discharge capacity of the alloy shows a maximum value with annealing temperature rising. Furthermore, the high rate discharge ability (HRD) first augments and then declines with the rising of Si content and annealing temperature.

Key words: A_2B_7-type electrode alloy; Si addition; annealing temperature; structure; electrochemical performances

1 Introduction

In 2009, the Ministry of Industry and Information Technology of China enacted "The regulation of access of new energy automobile production enterprises and products", in which hybrid electric vehicle (HEV) with nickel-metal hydride battery as auxiliary power has been classified as a mature product for nationwide selling, which provides a golden opportunity for the development of the Ni/MH battery. A series of metal hydride materials such as the rare-earth-based AB_5-type alloys[1], the AB_2-type Laves phase alloys[2], the V-based solid solution alloys[3] and the Mg-based alloys[4,5], are viewed as potential electrode materials. In particular, the rare earth-based AB_5-type alloys have been industrialized in large scale in China and Japan. However, there is still no perfect choice among the above-mentioned hydrogen storage materials to meet the transport applications owing to the limitation of their properties, for instance, the low discharge capacity of the AB_5-type electrode alloy, the poor activation capability of the AB_2-type Laves phase as well as V-based solid solution electrode alloys and the poor cycle stability of the Mg-based electrode alloy. Hence, further improvements of these performances especially discharge capacity and electrochemical hydrogen storage kinetics are compulsory for Ni/MH batteries. In such circumstance, La-Mg-Ni-system A_2B_7-type alloys have been considered to be the most promising candidates as the negative electrode materials of Ni/MH rechargeable battery on account of their higher discharge capacities (380-410 $mAh \cdot g^{-1}$) and lower

(Received: Feb. 17, 2014; Accepted: Dec. 20, 2014)

ZHANG Yanghuan(张羊换): Prof.; Ph D; E-mail: zhangyh59@sina.com

Funded by National Natural Science Foundations of China (Nos.51161015 and 51371094), National 863 Plans Projects of China (No.2011AA03A408)

production costs since Kadir *et al*[6] and Kohno *et al*[7] reported their research results. As a matter of fact, the National High Technology Research and Development Program of China ("863" Program for short) has provided a huge number of financial supports in order to promote the industrialization of these new-type alloys. Although, dramatic progress has been achieved as summarized by Liu *et al*[8,9], the production of the new type alloys as the negative electrode in Ni/MH battery has not been found in China yet by virtue of their rather poor electrochemical cycle stability. So how to enhance the cycle stability of the alloy without reducing its discharge capacity is still a serious challenge faced by these researchers.

As was well-known, the capacity deterioration of the La-Mg-Ni system alloy electrodes is mainly attributed to the pulverization of the alloy particles and the oxidation/corrosion of the elements Mg and La[9]. Usually, the element substitution or addition is an effective method of improving the overall properties of the hydrogen storage alloys. In addition, the fabrication technology is also extremely vital to ameliorating the performances. In a previous investigation of the ternary system, we studied the effect of annealing on the cycle stability of the alloy electrodes in detail. The results showed that annealing treatment significantly changes the structures and phase compositions of the alloy, enhancing the anti-pulverization and anti-corrosion and improving the cycle stability of the alloy electrodes observably[10,11]. Hence, it is expected that the combination of an optimized amount of additive Si with proper annealing technology may yield an alloy with superior electrochemical performances. To validate this, a systematical investigation about the effects of Si content and annealing temperature on the structures and electrochemical hydrogen storage performances of the $La_{0.8}Mg_{0.2}Ni_{3.3}Co_{0.2}Si_x$ (x = 0-0.2) electrode alloys has been conducted.

2 Experimental

The chemical compositions of the electrode alloys were $La_{0.8}Mg_{0.2}Ni_{3.3}Co_{0.2}Si_x$ (x = 0-0.2). For convenience, the alloys were denoted with Si content as Si_0, $Si_{0.05}$, $Si_{0.1}$, $Si_{0.15}$ and $Si_{0.2}$, respectively. The alloy ingots were prepared by using a vacuum induction furnace in a helium atmosphere under the pressure of 0.04 MPa in order to prevent element Mg from volatilizing during the melting. A part of the alloys were annealed at the temperatures of 900, 950, 1 000 and 1 050 ℃ for 8 h in vacuum.

The phase structures and compositions of the as-cast and annealed alloys were characterized by XRD (D/max/2400). The morphologies of the as-cast and annealed alloys were examined by SEM (QUANTA 400).

The round electrode pellets with a 15 mm diameter were prepared by cold pressing the mixture of alloy powder and carbonyl nickel powder with a weight ratio of 1:4 under the pressure of 35 MPa. After dried for 4 h, the electrode pellets were immersed in a 6 mol•L^{-1} KOH solution for 24 h in order to wet the electrodes fully before the electrochemical measurement.

The electrochemical measurements were performed at 30 ℃ by using a tri-electrode open cell, consisting of a working electrode (the metal hydride electrode), a sintered $Ni(OH)_2$/NiOOH counter electrode and a Hg/HgO reference electrode, which were immersed in the electrolyte of 6 mol•L^{-1} KOH, defining the voltage between the negative electrode and the reference one as the discharge voltage. In every cycle, the alloy electrode was first charged with a constant current density. After resting for 15 min, it was discharged at the same current density to cut-off voltage of –0.500 V.

The electrochemical impedance spectra (EIS) and the Tafel polarization curves of the alloys were measured by electrochemical workstation (PARSTAT 2273). The fresh electrodes were fully charged and then rested for 2 h up to the open circuit potential stabilization. For the EIS measurement, the frequency range was from 10 kHz to 5 mHz at 50% depth of discharge (DOD), the amplitude of signal potentiostatic or galvanostatic measurements was 5 mV, the number of points per decade of frequencies was 60. The Tafel polarization curves were also recorded at 50% DOD, the potential range was –1.2 to +1.0 V (*vs* Hg/HgO) with a scan rate of 5 mV•s^{-1}. For the potentiostatic discharge, the test electrodes in the fully charged state were discharged at 500 mV potential steps for 5 000 s on electrochemical workstation (PARSTAT 2273), using the electrochemistry corrosion software (CorrWare).

3 Results and discussion

3.1 Structural characteristics

As shown in Fig.1, the XRD patterns of the as-cast and annealed $La_{0.8}Mg_{0.2}Ni_{3.3}Co_{0.2}Si_x$ (x = 0-0.2)

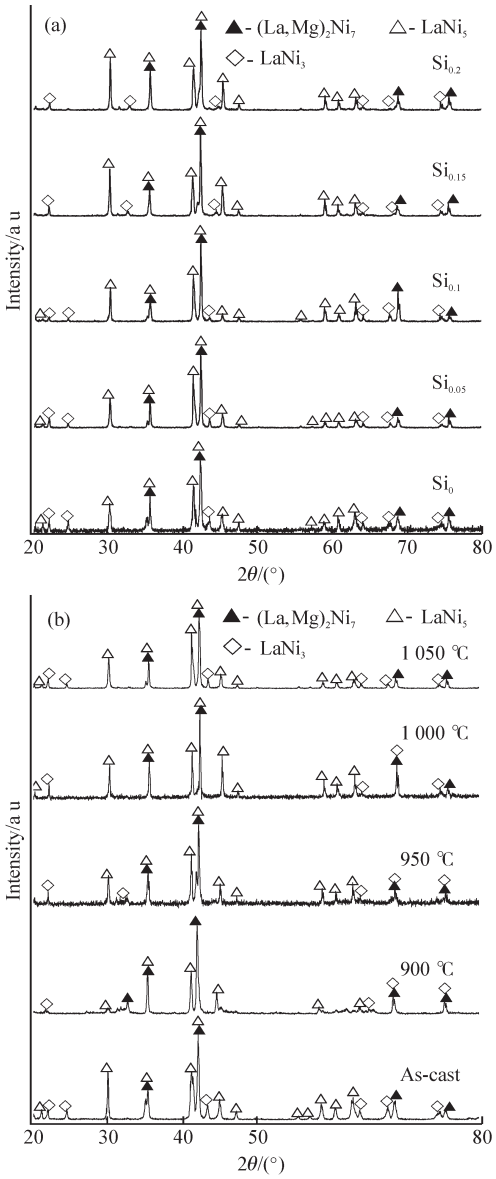

Fig.1 XRD patterns of the as-cast and annealed $La_{0.8}Mg_{0.2}Ni_{3.3}Co_{0.2}Si_x$ (x = 0-0.2) alloys: (a) As-annealed (1 050 ℃) alloy; (b) $Si_{0.05}$ alloy

alloys reveal that all the as-cast and annealed alloys are of a multiphase structure, containing two major phases $(La, Mg)_2Ni_7$ and $LaNi_5$ as well as a residual phase $LaNi_3$. Evidently, adding Si and the annealing treatment can hardly affect their phase component but change their phase abundances to a large extent. Listed in Tables 1 and 2 are the lattice parameters together with the abundances of the $(La, Mg)_2Ni_7$ and $LaNi_5$ major phases in the alloys, which were calculated by Jade 6.0 software based on the XRD data, from which it is found that the addition of Si makes the lattice constants and cell volumes of the two major phases enlarge notably, which justifies the successful alloying of Si with $(La, Mg)_2Ni_7$ and $LaNi_5$. Adding Si also makes the lattice constants of the $LaNi_5$ phase increase much larger than those of the $(La, Mg)_2Ni_7$ phase, implying that Si atoms prefer to form solid solution with the $LaNi_5$ phase. Besides, the addition of Si brings on an obvious decrease in the $(La, Mg)_2Ni_7$ phase and an increase in the $LaNi_5$ phase. Furthermore, Table 2 exhibits that the annealing treatment renders a slight increase in the lattice parameters and cell volume of the major phases in the alloys. The abundance of the $(La, Mg)_2Ni_7$ phase first increases and then decreases with increasing annealing temperature, while the $LaNi_5$ phase shows a completely opposite tendency, first decreasing and then increasing.

The SEM images of the as-cast and annealed Si_0 and $Si_{0.05}$ alloys are illustrated in Fig.2, from which it can be seen that the morphologies of the as-cast Si_0 and $Si_{0.05}$ alloys display a dendrite structure, which will vary obviously after being annealed, the grains of the alloys becoming very coarse. The analysis of SEM equipped with an energy dispersive spectrometry (EDS) reveals that all the experimental alloys have multiphase structure, containing $(La, Mg)_2Ni_7$ (denoted as A), $LaNi_5$ (denoted as B) as well as $LaNi_3$ (denoted

Table 1 Lattice parameters and abundances of $(La, Mg)_2Ni_7$ and $LaNi_5$ major phases of the as-annealed (1 050 ℃) alloys

Alloys	Major phases	Lattice constants a/nm	c/nm	Cell volumes V/nm^3	Phase abundance/wt%
Si_0	$(La, Mg)_2Ni_7$				
	$LaNi_5$	0.506 8	2.457 2	0.546 6	68.2
$Si_{0.05}$	$(La, Mg)_2Ni_7$	0.504 4	0.401 1	0.088 4	28.3
	LaNi5	0.506 9	2.457 3	0.546 8	66.5
$Si_{0.1}$	$(La, Mg)_2Ni_7$	0.504 9	0.401 6	0.088 7	29.8
	$LaNi_5$	0.506 9	2.457 4	0.546 8	63.1
$Si_{0.15}$	$(La, Mg)_2Ni_7$	0.505 3	0.402 1	0.088 9	32.1
	$LaNi_5$	0.507 0	2.457 5	0.547 1	57.6
$Si_{0.2}$	$(La, Mg)_2Ni_7$	0.505 9	0.402 6	0.089 2	38.1
	$LaNi_5$	0.507 0	2.457 6	0.547 1	52.5
		0.506 3	0.403 0	0.089 5	42.9

Table 2 Lattice parameters and abundances of $(La, Mg)_2Ni_7$ and $LaNi_5$ major phases of the $Si_{0.05}$ alloys annealed at different temperature

Annealing temperature/℃	Major phases	Lattice constants *a*/nm	*c*/nm	Cell volumes *V*/nm^3	Phase abundance /wt%
As-cast	$(La, Mg)_2Ni_7$	0.506 3	2.456 8	0.545 4	70.1
	$LaNi_5$	0.504 2	0.400 9	0.088 3	25.2
900	$(La, Mg)_2Ni_7$	0.506 5	2.457 0	0.545 9	73.1
	$LaNi_5$	0.504 4	0.401 2	0.088 4	22.2
950	$(La, Mg)_2Ni_7$	0.506 6	2.457 1	0.546 1	72.1
	$LaNi_5$	0.504 6	0.401 3	0.088 5	23.0
1 000	$(La, Mg)_2Ni_7$	0.506 7	2.457 3	0.546 4	68.3
	$LaNi_5$	0.504 8	0.401 5	0.088 6	27.2
1 050	$(La, Mg)_2Ni_7$	0.506 9	2.457 3	0.546 8	66.5
	$LaNi_5$	0.504 9	0.401 6	0.088 7	29.8

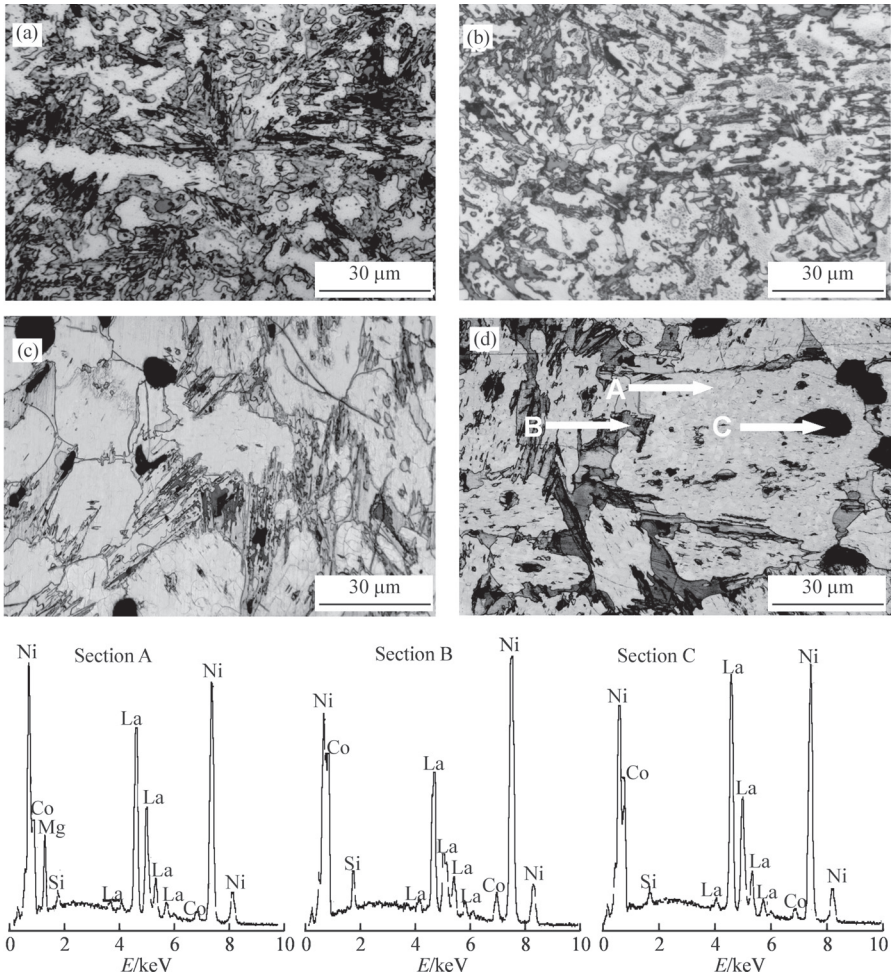

Fig.2 (a-d) SEM images of the as-cast and annealed alloys and typical EDS spectra of sections A, B and C in (d): (a) As-cast Si_0 alloy; (b) As-cast $Si_{0.05}$ alloy; (c) As-annealed (1 050 ℃) Si_0 alloy; (d) As-annealed (1 050 ℃) $Si_{0.05}$ alloy

as C) phase. The EDS patterns also show that Si concentration in the $LaNi_5$ phase is clearly higher than that in $(La, Mg)_2Ni_7$ phase, which corresponds well with the results of the XRD observation.

3.2 Electrochemical hydrogen storage performances

3.2.1 Discharge capacity

Fig.3 provides the variations of the discharge potentials of the as-cast and annealed $La_{0.8}Mg_{0.2}Ni_{3.3}Co_{0.2}Si_x$ (x = 0-0.2) alloys with the discharge capacity varying. Evidently, the discharge potential characteristic, which is directly related to the stability of the output power, is an extremely important performance of the alloy electrode and is characterized by the potential plateau of the discharge curve of the alloy. The longer and the more horizontal the discharge

potential plateau is, the better the discharge potential characteristics of the alloy will be. It can be seen from Fig.3 that all the discharge potentials of the alloys have a long potential plateau during the discharge process, which means that the output power of the battery is very stable. The addition of Si and annealing treatment does not seem to play a significant role in affecting the potential plateau of the alloy electrodes.

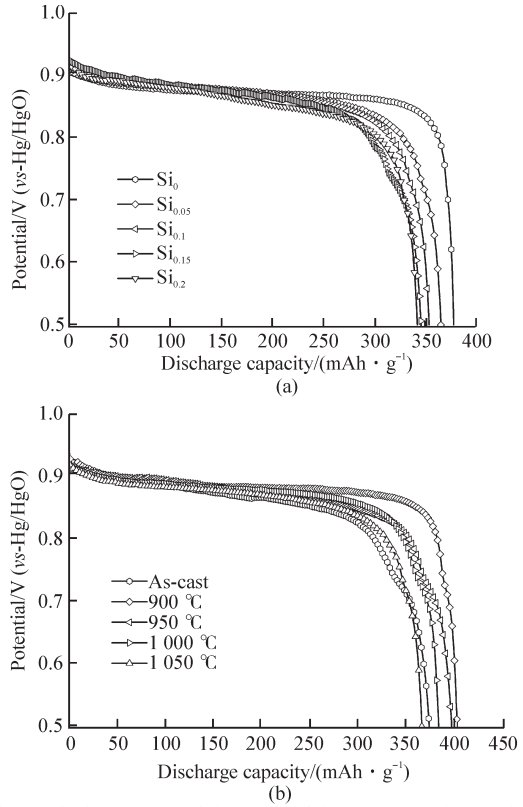

Fig.3 Discharge potential curves of the as-cast and annealed $La_{0.8}Mg_{0.2}Ni_{3.3}Co_{0.2}Si_x$ (x = 0-0.2) alloys: (a) As-annealed (1 050 ℃) alloy; (b) $Si_{0.05}$ alloy

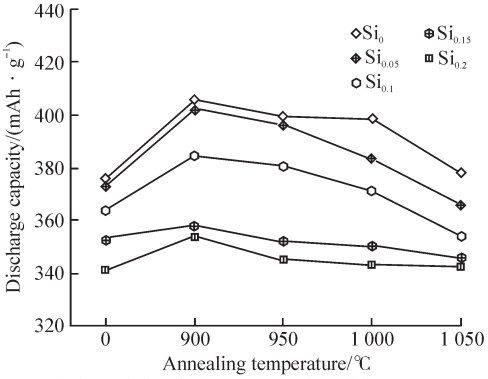

Fig.4 Evolution of the discharge capacity of the $La_{0.8}Mg_{0.2}Ni_{3.3}Co_{0.2}Si_x$ (x = 0-0.2) alloys with annealing temperature

The discharge capacity of the as-cast and annealed $La_{0.8}Mg_{0.2}Ni_{3.3}Co_{0.2}Si_x$ (x = 0-0.2) alloys as a function of the annealing temperature is described in Fig.4. It is evident that the discharge capacity of alloy first grows and then declines with annealing temperature rising. When annealed at 900 °C, the Si_0, $Si_{0.05}$, $Si_{0.1}$, $Si_{0.15}$ and $Si_{0.2}$ alloys all yield the maximum discharge capacities of 405.5, 402.3, 384.8, 357.9 and 354.1 mAh•g^{-1}, respectively. Evidently, it can be seen from Fig.4 that whatever state is, the discharge capacity of the alloy decreases with Si content rising. The discharge capacity is reduced from 375.5 to 341.6 mAh•g^{-1} for the as-cast alloy and from 405.5 to 354.1 mAh•g^{-1} for the as-annealed (900 ℃) alloy by increasing Si content from 0 to 0.2.

The alloy with the maximum discharge capacity is basically attributed to the change of the phase abundance of the alloy incurred by annealing treatment. When annealed at 900 ℃, the abundance of $(La, Mg)_2Ni_7$ phase increases and the cell volume becomes enlarged, which facilitates to enhance the discharge capacity. When the temperature is higher than 900 ℃, the annealing brings about a decrease in the $(La, Mg)_2Ni_7$ phase and an increase in the $LaNi_5$ phase, which accordingly engenders the decline of the discharge capacity since the $(La, Mg)_2Ni_7$ phase possesses much higher electrochemical capacity than that of the $LaNi_5$ phase. As regards to the decreased discharge capacity incurred by adding Si, it is ascribed to two aspects. On the one hand, the addition of Si plays a negative role on the discharge capacity of $LaNi_5$ phase, which is universally convinced[12,13]. On the other hand, the reduction of the $(La, Mg)_2Ni_7$ phase resulted from adding Si is harmful to the discharge capacity of the alloy.

3.2.2 Cycle stability

The cycle life of the electrode alloy is viewed as a decisive factor for the application of the Ni/MH battery, which is characterized by the cycle number when the discharge capacity is reduced to 60% of the maximum capacity. The evolution of discharge capacity of the as-cast and annealed $La_{0.8}Mg_{0.2}Ni_{3.3}Co_{0.2}Si_x$ (x = 0-0.2) alloys with cycle number is described in Fig.5, from which the process of the capacity degradation can be seen clearly. The slopes of the curves qualitatively reflect the degradation rate of the discharge capacity during the charge-discharge cycle, namely the smaller the slope of the curve is, the better the cycle life of the alloy will be. In respect of the degradation rate of the discharge capacity, it clearly falls with the Si content growing, indicating that the addition of Si plays a positive impact on the cycle life of the alloy electrode. At the same time, it can be found from Fig.5 (b) that the degradation rate of the discharge capacity of the $Si_{0.05}$ alloy first goes down and then mounts up with

the annealing temperature increasing, suggesting the existence of an optimal annealing temperature. In order to respectively establish the relationship between the cycle stability of the alloy and Si content as well as the cycle stability and annealing temperature, the capacity retaining rate (S_{100}) is introduced to accurately evaluate the cycle stability of the alloy, which is defined as $S_{100} = C_{100}/C_{max}\times100\%$, where C_{max} is the maximum discharge capacity and C_{100} is the discharge capacity at the 100th cycle with a current density of 300 mA•g^{-1}, respectively. Here, the variations of the S_{100} values of the $La_{0.8}Mg_{0.2}Ni_{3.3}Co_{0.2}Si_x$ (x = 0-0.2) alloys with Si content as well as annealing temperature are also inserted in Fig.5. Clearly, it is found that the S_{100} values of the as-annealed (1 050 ℃) alloys grow with the rising of Si content, being enhanced from 78.7% to 85.8% by increasing Si content from 0 to 0.2. Likewise, the S_{100} value of the $Si_{0.05}$ alloy also clearly augments with the annealing temperature rising 1 000 ℃, but when the temperature reaches 1 050 ℃, an undesired decline appears, namely the S_{100} value first rises from 68.9% to 85.6% and then decreases to 81.5% at last.

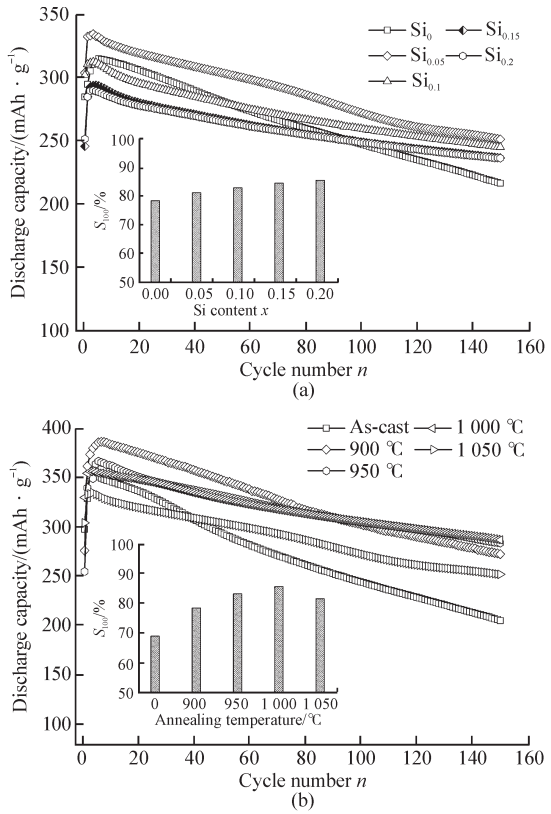

Fig.5 Evolution of the discharge capacity of the $La_{0.8}Mg_{0.2}Ni_{3.3}Co_{0.2}Si_x$ (x = 0-0.2) alloys with cycle number: (a) As-annealed (1 050 ℃) alloy; (b) $Si_{0.05}$ alloy

Usually, the invalidation of an electrode is characterized by the decay of discharge capacity and the drop of discharge voltage[14]. It has been ascertained that the degradation of the discharge capacity of the A_2B_7-type alloy electrode principally results from the forming and ever-thickening of $Mg(OH)_2$ and $La(OH)_3$ surface layers which hinder the hydrogen atoms from diffusing in or out, in alkaline solutions[15]. Besides, the hydrogen storage alloy suffers from a volume change during the charge-discharge process which inevitably aggravates the cracking and pulverization of the alloy, consequently making the surface of the alloy easy to be oxidized. Generally, the positive contribution of the additive Si on the cycle stability of the alloy is associated with the following aspects. Firstly, the addition of Si facilitates forming a compact silicon oxide layer on the surface of the alloy electrode[1,16] which prevents it from being corroded effectively. Secondly, the enlarged cell volume caused by adding Si reduces the ratios of expansion/contraction in the process of hydrogen absorption/desorption, enhancing the anti-pulverization capability. What is more, the $LaNi_5$ phase increased by adding Si plays a beneficial role on the cycle stability due to an inarguable fact that the cycle stability of the $LaNi_5$ phase is greatly superior to that of the $(La, Mg)_2Ni_7$ phase. Subsequently, we discuss the effect of annealing treatment. The $Si_{0.05}$ alloy yields a maximum S_{100} value with annealing temperature growing as shown in Fig.5 (b), suggesting that the annealing treatment engenders beneficial and harmful impacts on the cycle stability of the alloy simultaneously. The beneficial aspect is ascribed to the enlarged cell volumes and more homogeneous composition distribution resulted from annealing, which facilitate to inhibit the pulverization of the alloy, improving the cycle stability of the alloy. The harmful side is due to the coarsened grains generated by annealing. As considered by Sakai *et al*[17], a passivation layer forming on the grain boundaries could exert an effectively protective action until the alloy was pulverized below the grain size. Hence, it is convinced that the alloy with the smaller grain size has better cycle stability.

3.2.3 Electrochemical hydrogen storage kinetics

The electrochemical hydrogen storage kinetics of an alloy electrode is evaluated by its high rate discharge ability (HRD), which is defined as: HRD = $C_{600,max}/C_{60,max}\times100\%$, where $C_{600,max}$ and $C_{60,max}$ are the maximum discharge capacities of the alloy electrode charged-discharged at the current densities of 600 and 60 mA•g^{-1}, respectively. The variations of HRD values of the as-cast and annealed $La_{0.8}Mg_{0.2}Ni_{3.3}Co_{0.2}Si_x$ (x

= 0-0.2) alloys with the annealing temperature are exhibited in Fig.6, from which it is found that the HRD values of all the alloys except Si_0 alloy show maximum values with annealing temperature rising, which are 90.3%, 87.3%, 85.3% and 84.1% corresponding to the $Si_{0.05}$, $Si_{0.1}$, $Si_{0.15}$ and $Si_{0.2}$ alloys, respectively.

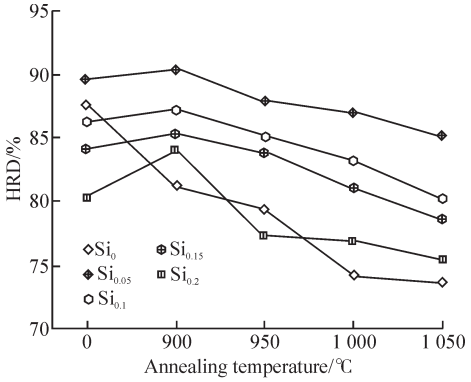

Fig.6 Evolution of the HRD of the $La_{0.8}Mg_{0.2}Ni_{3.3}Co_{0.2}Si_x$ (x = 0-0.2) alloys with annealing temperature

The electrochemical hydriding/dehydriding reaction taking place at the hydrogen storage electrode in an alkaline solution during charging and discharging process can be summarized as follows:

$$M+\frac{x}{2}H_2O+\frac{x}{2}e^- \leftrightarrow MH_x+\frac{x}{2}OH^- \quad (1)$$

where M is the hydrogen storage alloy. It can be seen from the above equation that when the alloy electrode is charging in KOH solution, hydrogen atoms originating from electrolyzing H_2O diffuse from the interface between the alloy and electrolyte into the bulk alloy and then store them in the metallic lattice in the form of hydride. In the process of discharging, the hydrogen stored in the bulk alloy diffuses toward the surface where it is oxidized. The hydrogen atoms adhering to the grain surface of the alloy electrode will go to two possible destinations, forming hydrogen molecule or diffusing into the bulk alloy where they exist in the form of hydride. This means that the diffusion rate of hydrogen atoms on the surface layer of alloy is just the ratio of the diffusion current to the imposed current, which is a vital factor to determine the utilization of charging current. That is to say, the electrochemical hydrogen storage kinetics of the alloy electrode is determined by the charge-transfer rate on the surface of an alloy electrode and the hydrogen diffusion capability in the alloy bulk[18]. Thereby, it is extremely necessary to investigate the hydrogen diffusion coefficient and the charge-transfer rate.

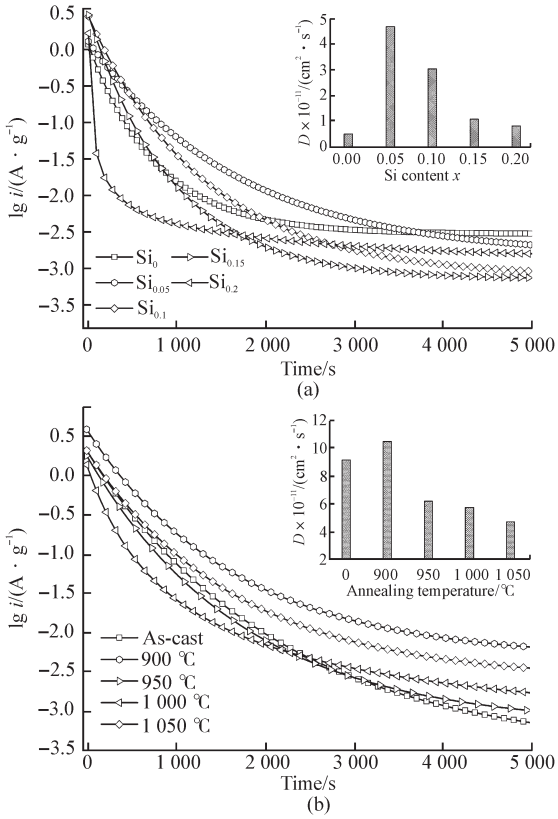

Fig.7 Semilogarithmic curves of anodic current *vs* time responses of the as-cast and annealed $La_{0.8}Mg_{0.2}Ni_{3.3}Co_{0.2}Si_x$ (x =0-0.2) alloys: (a) As-annealed (1 050 ℃) alloy, (b) $Si_{0.05}$ alloy

Based on the model built by White *et al*[19], the diffusion coefficients of hydrogen atoms can be obtained by measuring the semilogarithmic curves of anodic current versus working duration of an alloy, the results of the as-cast and annealed $La_{0.8}Mg_{0.2}Ni_{3.3}Co_{0.2}Si_x$ (x = 0-0.2) alloys are presented in Fig.7. The diffusion coefficient of the hydrogen atoms in the alloy bulk could be calculated through the slope of the linear region of the corresponding plots by the following formulae:

$$\log i=\log\left(\pm\frac{6FD}{da^2}(C_0-C_s)\right)-\frac{\pi^2}{2.303}\frac{D}{a^2}t \quad (2)$$

$$D=-\frac{2.303a^2}{\pi^2}\frac{\mathrm{d}\log i}{\mathrm{d}t} \quad (3)$$

where i is the diffusion current density ($A\cdot g^{-1}$), F is the Faraday constant, D is the hydrogen diffusion coefficient ($cm^2\cdot s^{-1}$), C_0 is the initial hydrogen concentration in the bulk of the alloy ($mol\cdot cm^{-3}$), C_s is the hydrogen concentration on the surface of the alloy particles ($mol\cdot cm^{-3}$), a is the alloy particle radius (cm), d is the density of the hydrogen storage alloy ($g\cdot cm^{-3}$), and t is the discharge time (s), respectively. The variations of the D values of the as-cast and annealed

alloys depending on the Si content and the annealing temperature are also provided in Fig.7. Clearly, the *D* values of the alloys first augment and then decline with the rising of the Si content and the annealing temperature, which corresponds well with the results in Fig.6.

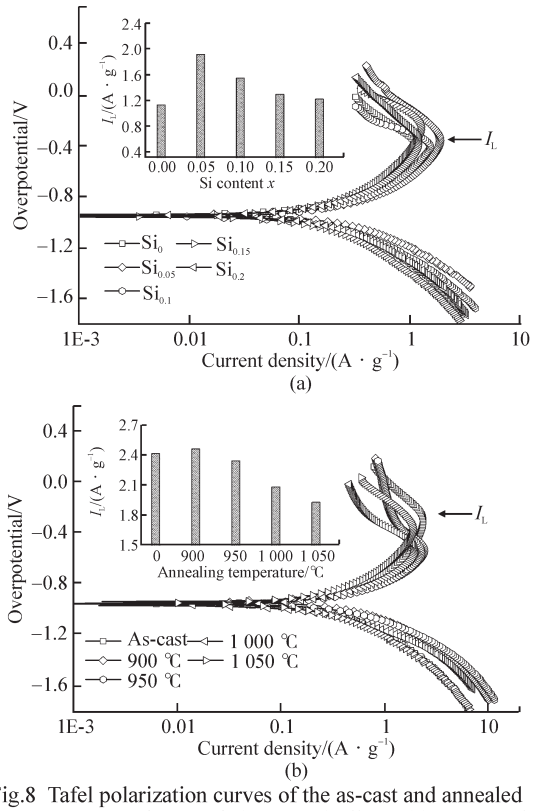

Fig.8 Tafel polarization curves of the as-cast and annealed $La_{0.8}Mg_{0.2}Ni_{3.3}Co_{0.2}Si_x$ (x = 0-0.2) alloys: (a) As-annealed (1 050 ℃) alloy; (b) $Si_{0.05}$ alloy

Fig.8 displays the Tafel polarization curve of the as-cast and annealed $La_{0.8}Mg_{0.2}Ni_{3.3}Co_{0.2}Si_x$ (x = 0-0.2) alloys. It can be seen that, in all cases, there is a clear point of inflection in each anodic polarization curve, implying the presence of critical value which is termed as limiting current density (I_L). It means that an oxidation reaction takes place on the surface of the alloy electrode and the oxidation layer hinders hydrogen atoms from further penetrating[20]. Hence, the limiting current density (I_L) can be viewed as a critical current density of passivation, basically depending on the diffusion rate of hydrogen in alloy electrode[18]. The variations of the I_L values of the alloys with the Si content and the annealing temperature are also provided in Fig.8. We note that the I_L values of the alloys first mount up and then go down with the growing of the Si content and the annealing temperature.

In terms of the charge-transfer ability on the surface of an alloy electrode, it can be qualitatively evaluated by its electrochemical impedance spectrum (EIS), as interpreted and modeled by Kuriyama *et al*[21]. The EIS curves of the as-cast and annealed $La_{0.8}Mg_{0.2}Ni_{3.3}Co_{0.2}Si_x$ (x = 0-0.2) alloys are illustrated in Fig.9. Clearly, we find that each EIS spectrum contains two distorted capacitive loops at high and middle frequencies as well as an almost straight line at low frequency. The smaller semicircle in the high frequency region signifies the contact resistance between the alloy powder and the conductive material, and the larger one in the middle frequency region symbolizes the charge-transfer resistance on the alloy surface, while the line at low frequency emblematizes the atomic hydrogen diffusion in the alloy. Thereby, it seems to be self-evident that the larger the radius of the semicircle in the middle frequency region is, the higher the charge-transfer resistance of the alloy electrode will be. Apparently, the radii of the large semicircles of the alloys in the middle frequency first shrink and then expand with the rising of Si content and the annealing temperature. In summary, based on the above-mentioned results, we can conclude that the high rate discharge ability (HRD) of the experimental alloys is dominated by the charge-transfer rate and the hydrogen diffusion capability jointly.

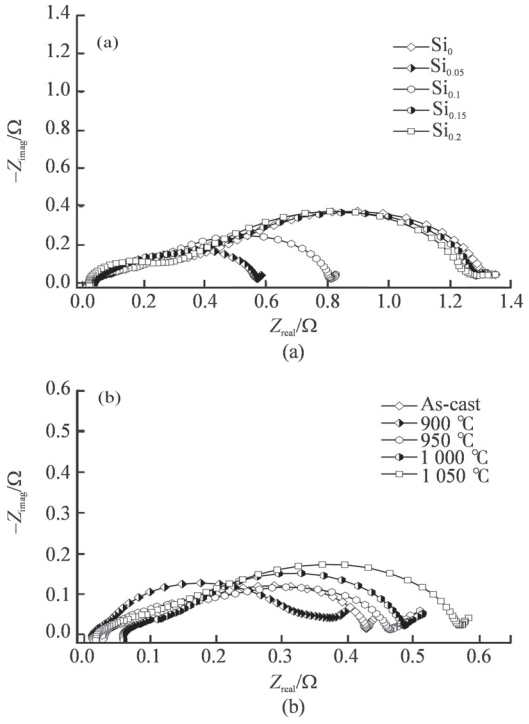

Fig.9 Electrochemical impedance spectra (EIS) of the as-cast and annealed $La_{0.8}Mg_{0.2}Ni_{3.3}Co_{0.2}Si_x$ (x = 0-0.2) alloys: (a) As-annealed (1 050 ℃) alloy; (b) $Si_{0.05}$ alloy

In general, the measurements of the HRD, EIS, limiting current density (I_L) and hydrogen diffusion coefficient (D) all exhibit that the electrochemical kinetics of all the alloys first augment and then fall

with the rising of the Si content and the annealing temperature except Si_0, implying that both the adding Si and the annealing treatment bring about positive and negative impacts on the electrode hydrogen storage kinetics. Here we will first discuss the actions of adding Si. The beneficial contribution is affiliated with two aspects: on one hand, the enlarged cell volume incurred by adding Si reduces diffusion activation energy of hydrogen atoms; on the other hand, the $LaNi_5$ phase increased by adding Si ameliorates the electrocatalytic activity of the alloy electrodes dramatically. Contrarily, the compact silicon oxide layer created by adding Si not only severely impairs the charge-transfer rate on the alloy surface but also hinders the hydrogen diffusion from inner of the bulk to the surface of the alloy, consequently impairing the electrochemical kinetic property. As regards to the actions of the annealing treatment on the electrochemical kinetics, the positive contribution of the annealing treatment to the electrochemical kinetics is inarguably ascribed to the increased cell volumes induced by the annealing treatment, and its opposite action is credibly attributed to the coarsened grains resulted from the annealing. As considered by Cui *et al*[22], the increase of the lattice constants and cell volumes facilitates to reduce the diffusion activation energy of hydrogen atoms, thus enhancing hydrogen diffusion. Also, the diffusion ability of hydrogen atoms is very sensitive to grain size[23] because grain boundaries can provide many sites with low diffusing activation energy, aiding the diffusion of hydrogen atoms in alloys.

4 Conclusions

The addition of Si renders a visible enlargement in the lattice constants and cell volumes of the alloys. Also, such addition brings about an increase in the $LaNi_5$ phase and a decrease in the $(La, Mg)_2Ni_7$ phase without altering the major phase structures of the alloys. Furthermore, the addition of Si notably improves cycle stability of the alloy but simultaneously reduces the discharge capacity. Likewise, the annealing treatment leads to a clear enlargement in the lattice constants and cell volumes of the alloy. Also, the abundance of the $(La, Mg)_2Ni_7$ phase first grows and then declines with increasing annealing temperature, but the situation of $LaNi_5$ phase is quite the contrary. The annealing treatment obviously ameliorates the cycle stability of the alloy but makes the discharge capacity of the alloy first augment and then fall. The high rate discharge ability (HRD) of the Si-free alloy always declines with the annealing temperature rising, but those of the Si added alloys have a maximum value in the same case, with which a rather similar variation tendency is obtained by measuring the hydrogen diffusion coefficient (D), limiting current density (I_L) and electrochemical impedance spectra (EIS), suggesting that the high rate discharge ability (HRD) of the experimental alloys depends on the charge-transfer rate together with the hydrogen diffusion capability.

References

[1] Willems J J G, Buschow K H J. From Permanent Magnets to Rechargeable Hydride Electrodes[J]. *J. Less-Common. Met*., 1987, 129(1): 13-30

[2] Ovshinsky S R, Fetcenko M A, J Ross. A Nickel Metal Hydride Battery for Electric Vehicles[J]. *SCI*., 1993, 260: 176-181

[3] Tsukahara M, Kamiya T, Takahashi K, *et al*. Hydrogen Storage and Electrode Properties of V-based Solid Solution Type Alloys Prepared by a Thermic Process[J]. *J. Electrochem Soc*., 2000, 147(8): 2 941-2 944

[4] Sun D L, Enoki H, Gingl F, *et al*. New Approach for Synthesizing Mg-based Alloys[J]. *J. Alloys Compd.*, 1999, 285(1-2): 279-283

[5] Zhang Y H, Yang T, Shang H W, *et al*. Gaseous and Electrochemical Hydrogen Storage Kinetics of As-quenched Nanocrystalline and Amorphous Mg_2Ni-type Alloys[J]. *J. Wuhan University of Technology-Mater. Sci. Ed.*, 2013, 28(3): 604-611

[6] Kadir K, Sakai T, Uehara I. Synthesis and Structure Determination of a New Series of Hydrogen Storage Alloys; RMg_2Ni_9 (R = La, Ce, Pr, Nd, Sm and Gd) Built from $MgNi_2$ Laves-type Alternating with AB_5 Layers[J]. *J. Alloys Compd*., 1997, 257(1-2): 115-121

[7] Kohno T, Yoshida H, Kawashima F, *et al*. Hydrogen Storage Properties of New Ternary System Alloys: La_2MgNi_9, $La_5Mg_2Ni_{23}$, La_3MgNi_{14}[J]. *J. Alloys Compd.*, 2000, 311(2): L5-L7

[8] Liu Y F, Pan H G, Gao M X, *et al*. Advanced Hydrogen Storage Alloys for Ni/MH Rechargeable Batteries[J]. *J. Mater Chem*., 2011, 21(13): 4 743-4 755

[9] Liu Y F, Cao Y H, Huang L, *et al*. Rare Earth-Mg-Ni-based Hydrogen Storage Alloys as Negative Electrode Materials for Ni/MH Batteries[J]. *J. Alloys Compd*., 2011, 509(3): 675-686

[10] Zhang Y H, Hou Z H, Li B W, *et al*. An Investigation on Electrochemical Hydrogen Storage Performances of the As-cast and -annealed $La_{0.8-x}Sm_xMg_{0.2}Ni_{3.35}Al_{0.1}Si_{0.05}$ (x = 0-0.4) Alloys[J]. *J. Alloys Compd*., 2012, 537: 175-182

[11] Zhang Y H, Yang T, Shang H W, *et al*. Influence of Substituting La with Zr on Electrochemical Characteristics of As-spun RE-Mg-Ni-based A_2B_7-type Alloys[J]. *Advanced Materials Research*, 2012, 562-564: 72-76

[12] Sakai T, Oguro K, Miyamura H, *et al*. Some Factors Affecting the Cycle Lives of $LaNi_5$-based Alloy Electrodes of Hydrogen Batteries[J]. *J. Less-Common Met*., 1990, 161(2): 193-202

[13] Meli F, Zuettel A, Schlapbach L. Surface and Bulk Properties of $LaNi_{5-x}Si_x$ Alloys from the Viewpoint of Battery Applications[J]. *J. Alloys Compd.*, 1992, 190(1): 17-24

[14] Zhang Y H, Li B W, Ren H P, *et al*. Investigation on Structures and Electrochemical Performances of the As-cast and -quenched $La_{0.7}Mg_{0.3}Co_{0.45}Ni_{2.55-x}Fe_x$ (x = 0-0.4) Electrode Alloys[J]. *Int. J. Hydrogen Energy*, 2007, 32(18): 4 627-4 634

[15] Dornheim M, Doppiu S, Barkhordarian G, *et al*. Hydrogen Storage in Magnesium-based Hydrides and Hydride Composites[J]. *Scripta Mater*., 2007, 56(10): 841-846

[16] Willems J J G. Metal Hydride Electrodes Stability of $LaNi_5$-related Compounds[J]. *Philips J. Res*., 1984, 39: 1-94

[17] Sakai T, Hazama T, Miyamura H, *et al*. Rare-earth-based Alloy Electrodes for a Nickel-metal Hydride Battery[J]. *J. Less-Common Met*., 1991, 172-174: 1 175-1 184

[18] Ratnakumar B V, Witham C, Bowman R C, *et al*. Electrochemical Studies on $LaNi_{5-x}Sn_x$ Metal Hydride Alloy[J]. *J. Electrochem Soc*., 1996, 143(8): 2 578-2 584

[19] Zheng G, Popov B N, White R E, *et al*. Electrochemical Determination of the Diffusion Coefficient of Hydrogen Through an $LaNi_{4.25}Al_{0.75}$ Electrode in Alkaline Aqueous Solution[J]. *J. Electrochem. Soc*., 1995, 142(8): 2 695-2 698

[20] Zhao X Y, Ding Y, Ma L Q, *et al*. Electrochemical Properties of $MmNi_{3.8}Co_{0.75}Mn_{0.4}Al_{0.2}$ Hydrogen Storage Alloy Modified with Nanocrystalline Nickel[J]. *Int. J. Hydrogen Energy*, 2008, 33(22): 6 727-6 733

[21] Kuriyama N, Sakai T, Miyamura H, *et al*. Electrochemical Impedance and Deterioration Behavior of Metal Hydride Electrodes[J]. *J. Alloys Compd*., 1993, 202(1-2): 183-197

[22] Cui N, Luo J L. Electrochemical Study of Hydrogen Diffusion Behavior in Mg_2Ni-type Hydrogen Storage Alloy Electrodes[J]. *Int. J. Hydrogen Energy*, 1999, 24(1): 37-42

[23] Xie D H, Li P, Zeng C X, *et al*. Effect of Substitution of Nd for Mg on the Hydrogen Storage Properties of Mg_2Ni Alloy[J]. *J. Alloys Compd*., 2009, 478(1-2): 96-102